Electronic Supplementary information (ESI)

Sustainable polysaccharide-derived mesoporous carbons ("Starbon®") as additives in lithium-ion batteries negative electrodes: importance of the mesoporosity

Sanghoon Kim,[ab*] Angel Manuel Escamilla-Pérez,[a] Mario De Bruyn,[c] Johan G. Alauzun,[a] Nicolas Louvain,[b] Nicolas Brun,[a] Duncan Macquarrie,[c] Lorenzo Stievano,[b] Bruno Boury,[a] Laure Monconduit,[b] P. Hubert Mutin[a]

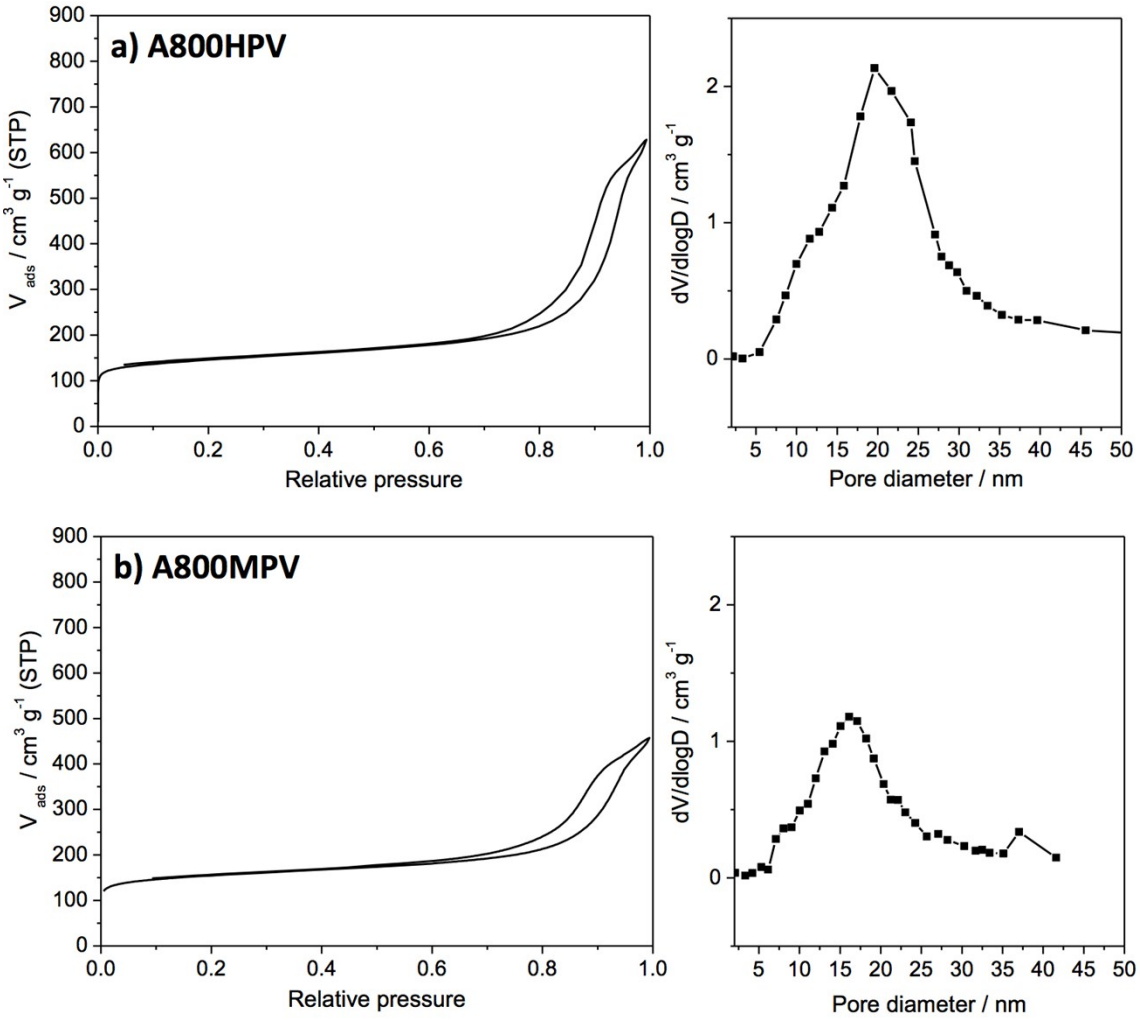

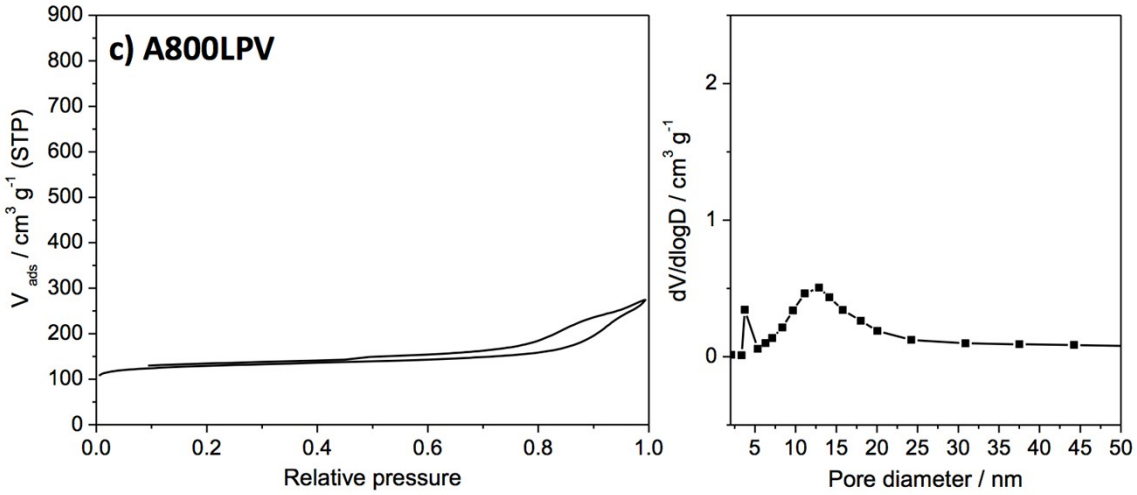
c) A800LPV
V ads / cm3 g-1 (STP)
Relative pressure
dV/dlogD / cm3 g-1
Pore diameter / nm

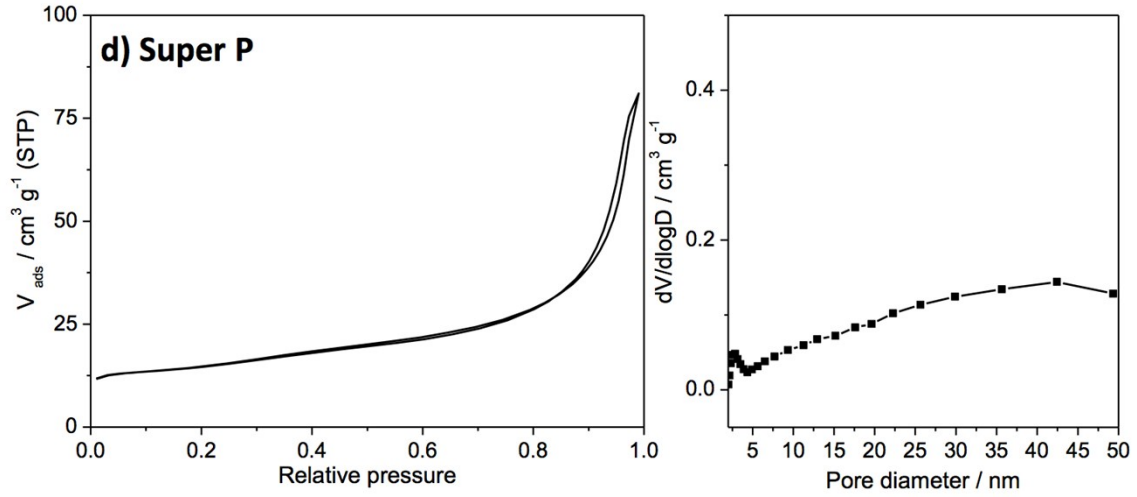
d) Super P
V ads / cm3 g-1 (STP)
Relative pressure
dV/dlogD / cm3 g-1
Pore diameter / nm

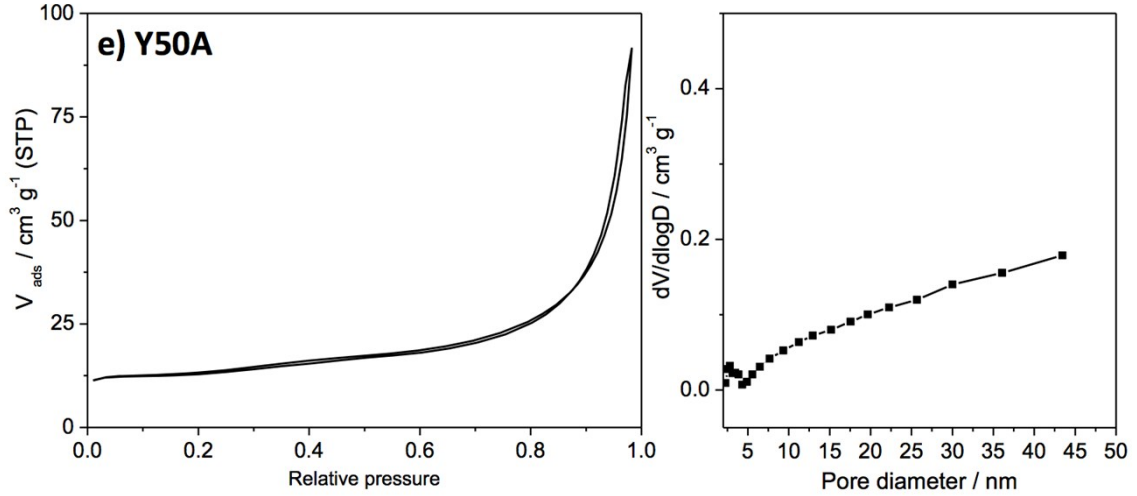
e) Y50A
V ads / cm3 g-1 (STP)
Relative pressure
dV/dlogD / cm3 g-1
Pore diameter / nm

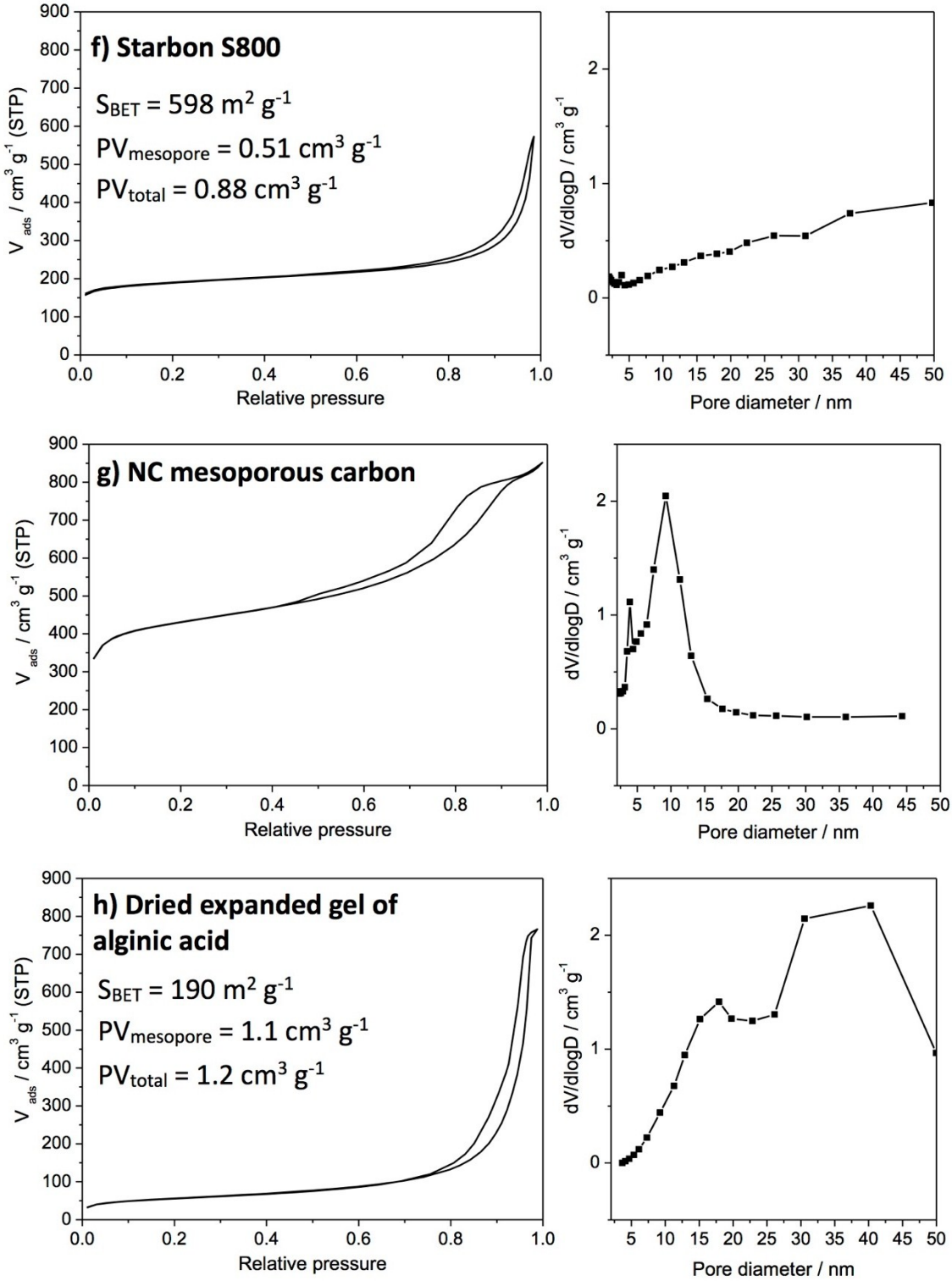

Fig. S1 N_2 adsorption-desorption isotherm and BJH pore size distribution (desorption branch) of a) A800HPV, b) A800MPV, c) A800LPV, d) Super P, e) Y50A, f) S800, g) NC mesoporous carbon and h) dried expanded gel of alginic acid, which was used as precursor for Starbon A800 materials.

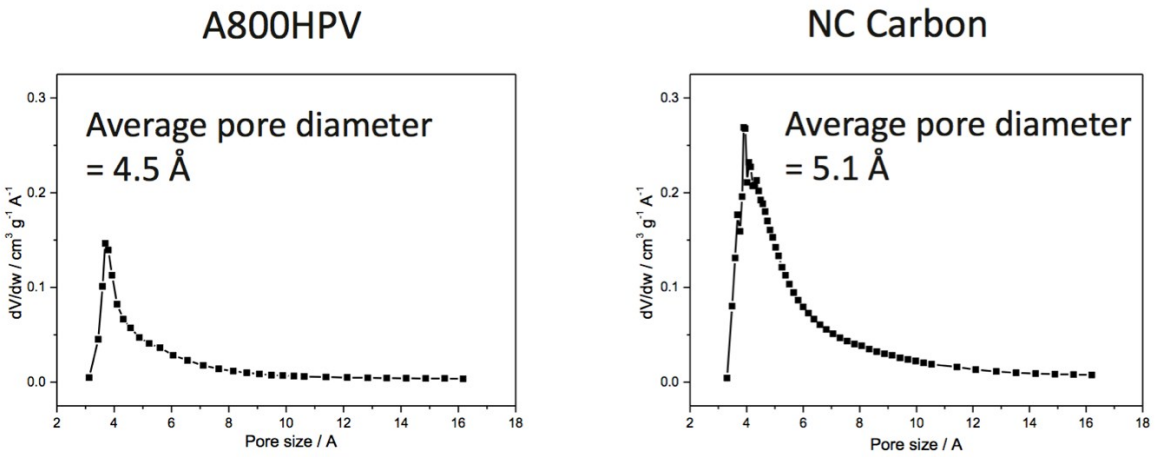

Fig. S2. Micropore size distribution of A800HPV and NC Carbon determined by Horvath-Kawazoe method (slit pores)

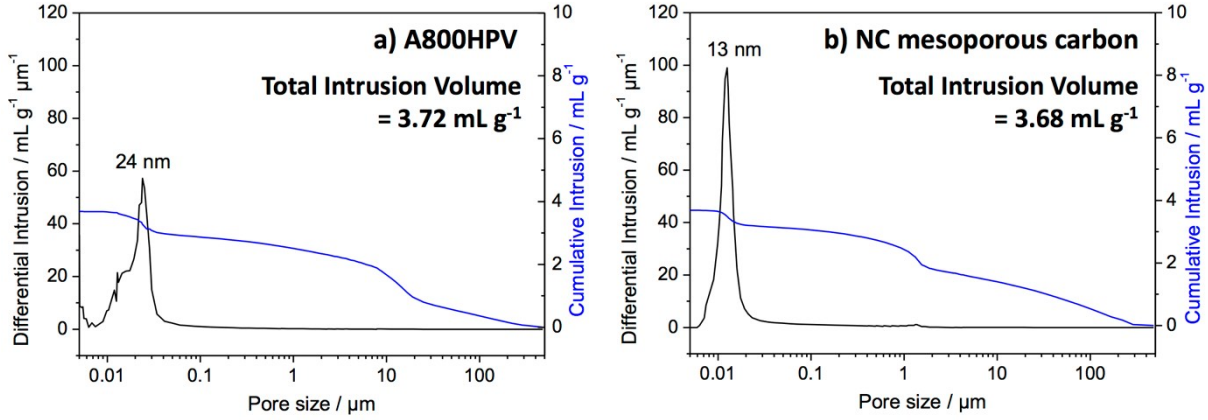

Fig. S3. Hg porosimetry data of a) A800HPV and b) NC mesoporous carbon.

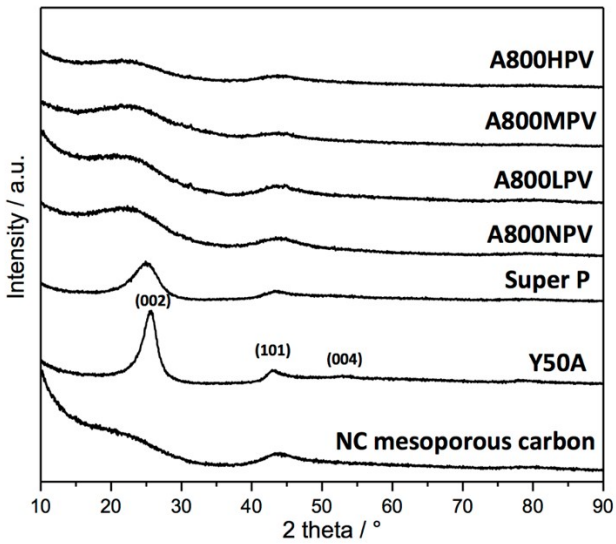

Fig. S4 Powder X-ray diffraction patterns of carbon additives used in this study. Peaks assignment was done only for Y50A, which exhibits clearly the diffraction peaks corresponding to (002), (101) and (004) planes of graphite.

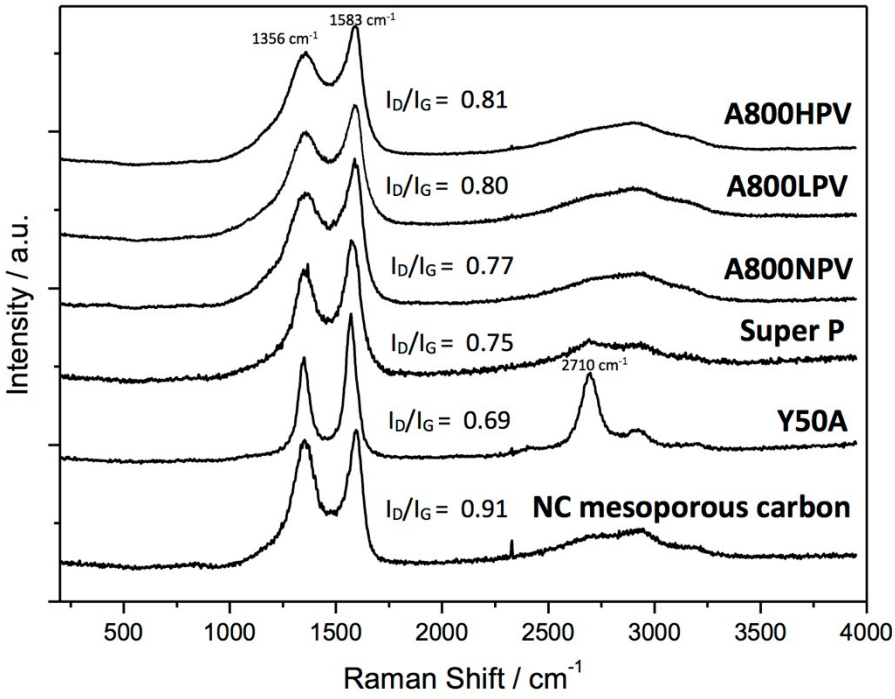

Fig. S5 Raman spectra of carbon additives used in this study. The ratio ID/IG calculated based on the intensity of D band (1350 cm^{-1}) and G band (1583 cm^{-1}). An intense peak at 2710 cm^{-1} for Y50A could indicate that this carbon additive is highly graphitized.

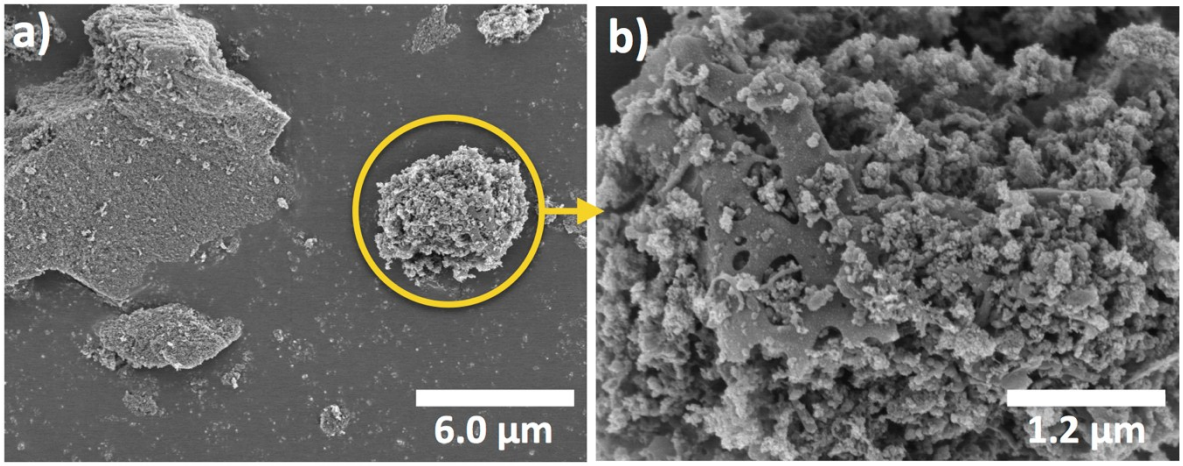

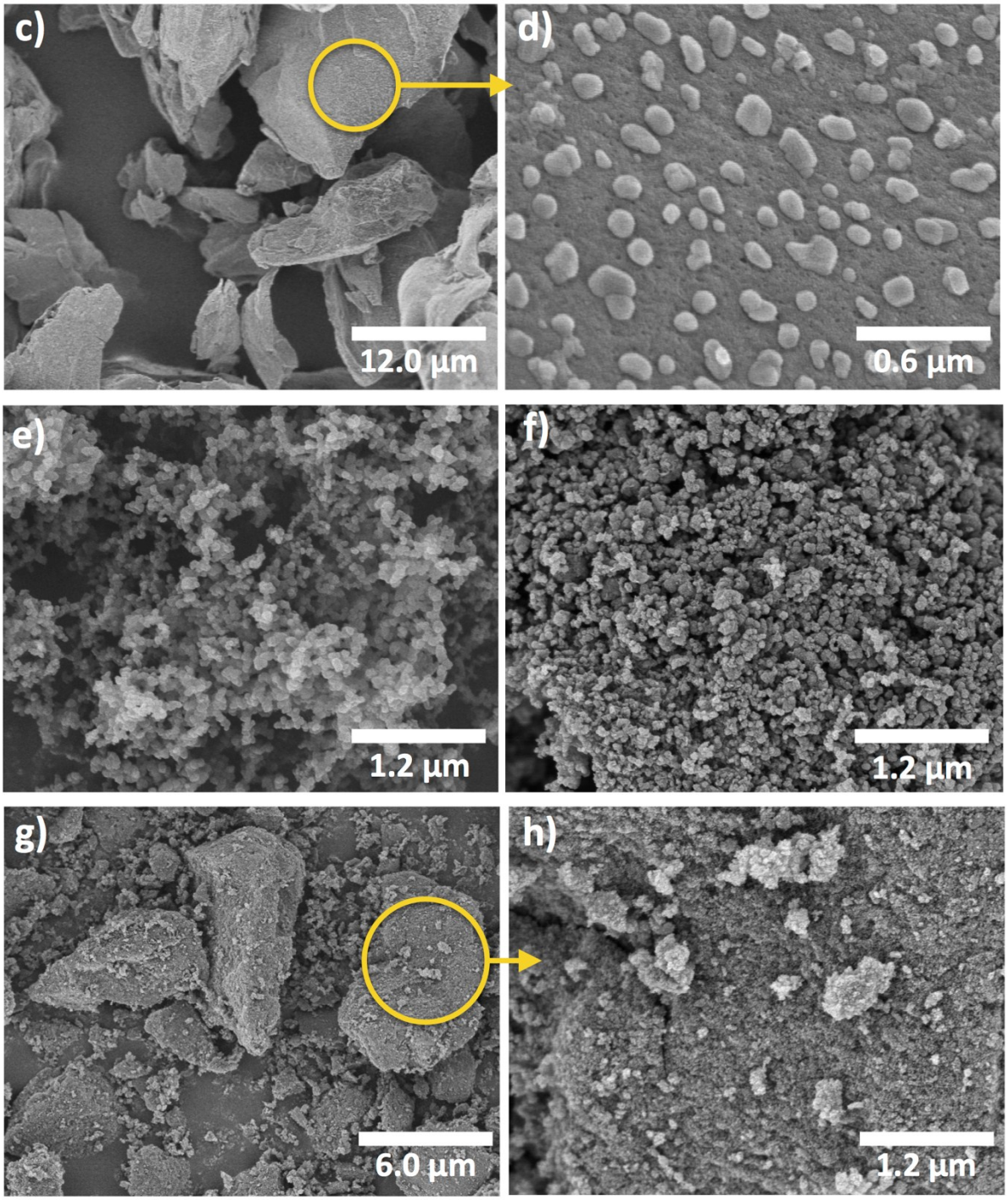

Fig. S6. SEM images of a) A800MPV, b) zoomed image of A800MPV, c) A800NPV, d) zoomed image of A800NPV, e) Super P, f) Y50A, g) NC mesoporous carbon, h) zoomed image of NC mesoporous carbon

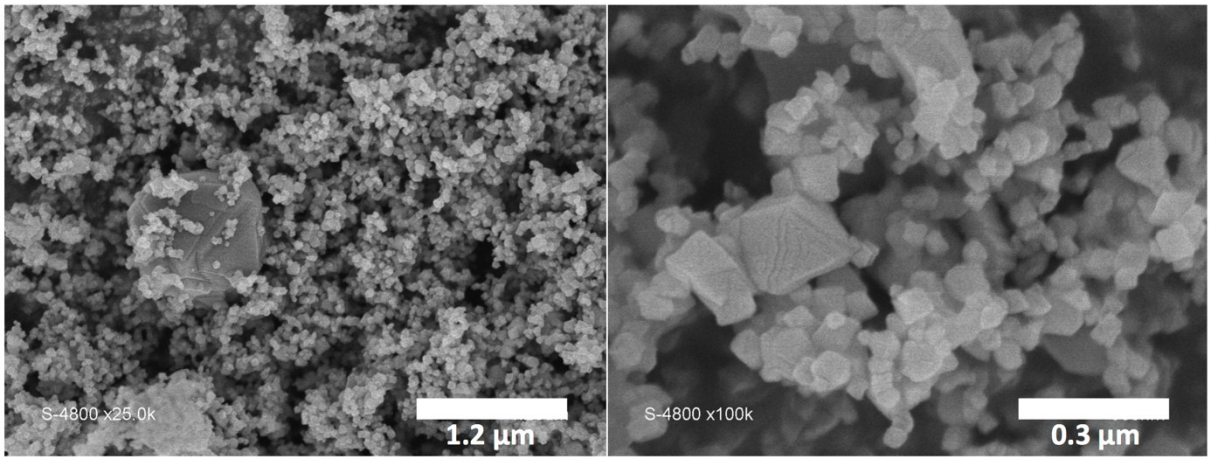

Fig. S7. SEM images of $Li_4Ti_5O_{12}$ (LTO) nanoparticles powder

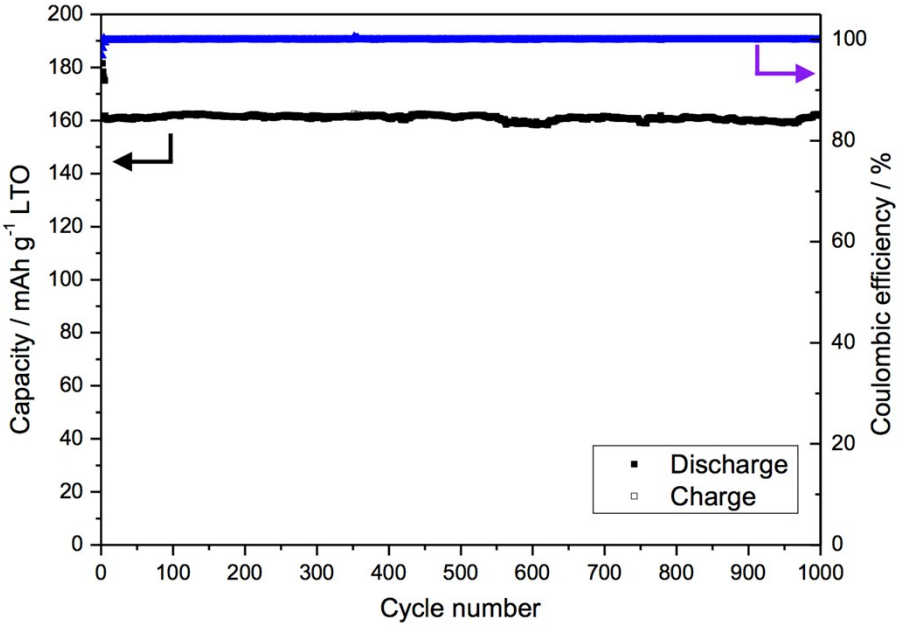

Fig. S8. Cyclic performance of LTO-A800HPV at 290 mA g-1. First 5 cycles were tested at 58 mA g^{-1}. No capacity fading was observed over 1000 cycles (162 mAh g^{-1} as the specific capacity of LTO).

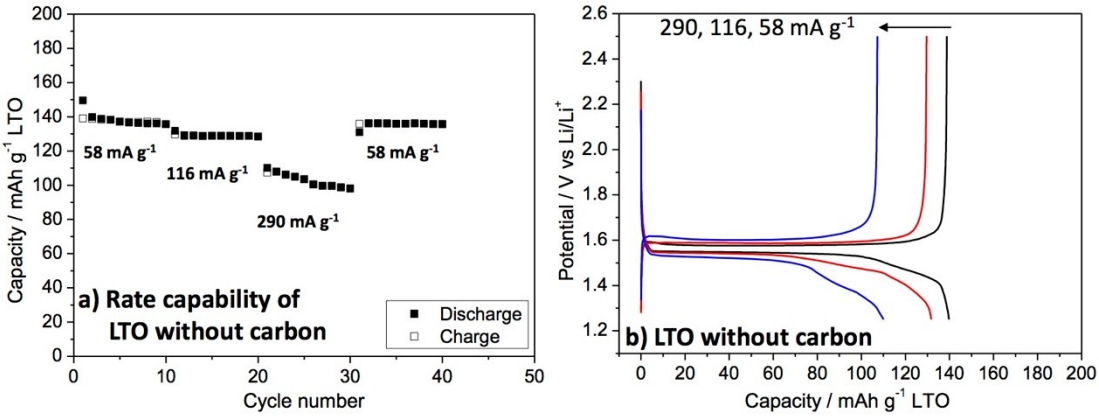

Fig. S9. Rate-capability and cyclic performance of a) LTO without any carbon additive and b) its galvanostatic charge-discharge voltage profile, which was performed only at 58, 116, 290 mA g^{-1}.

Current	58 mA g^{-1}	116 mA g^{-1}	290 mA g^{-1}	580 mA g^{-1}	Capacity retention (%)
LTO-A800HPV	177	171	163	154	87
LTO-A800MPV	157	155	147	126	80
LTO-A800LPV	140	144	124	105	75
LTO-A800NPV	127	116	102	73	57
LTO-Super P	157	149	143	130	83
LTO-Y50A	143	137	128	115	80
LTO-NC	160	152	146	132	83
LTO-A800HPV-14	171	167	160	144	84
LTO-A800HPV-10	169	165	158	140	83
LTO-A800HPV-3	162	158	150	133	82
LTO-A800LPV-14	141	135	127	117	83
LTO-S800	168	163	155	142	85

Table S1. Summary of the rate-capability of LTO electrodes. The amount of carbon additive is fixed at 6 wt.%, except mentioned otherwise, for example, LTO-A800HPV-14 stands for 14 wt.% of A800HPV used. Capacity retention (%) = Capacity at 580 mA g^{-1} / Capacity at 58 mA g^{-1}

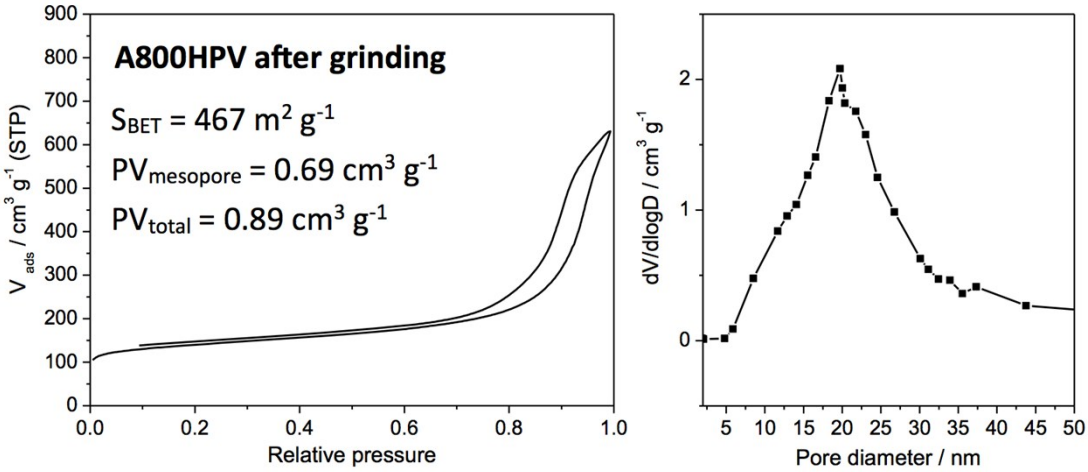

Fig. S10 N_2 physisorption isotherm and BJH pore size distribution (desorption branch) of A800HPV grinded using agate grinding jar at 500 rpm for 1 h. No change for S_{BET} and pore volume were observed, compared to the original A800HPV. (see also Fig S1)

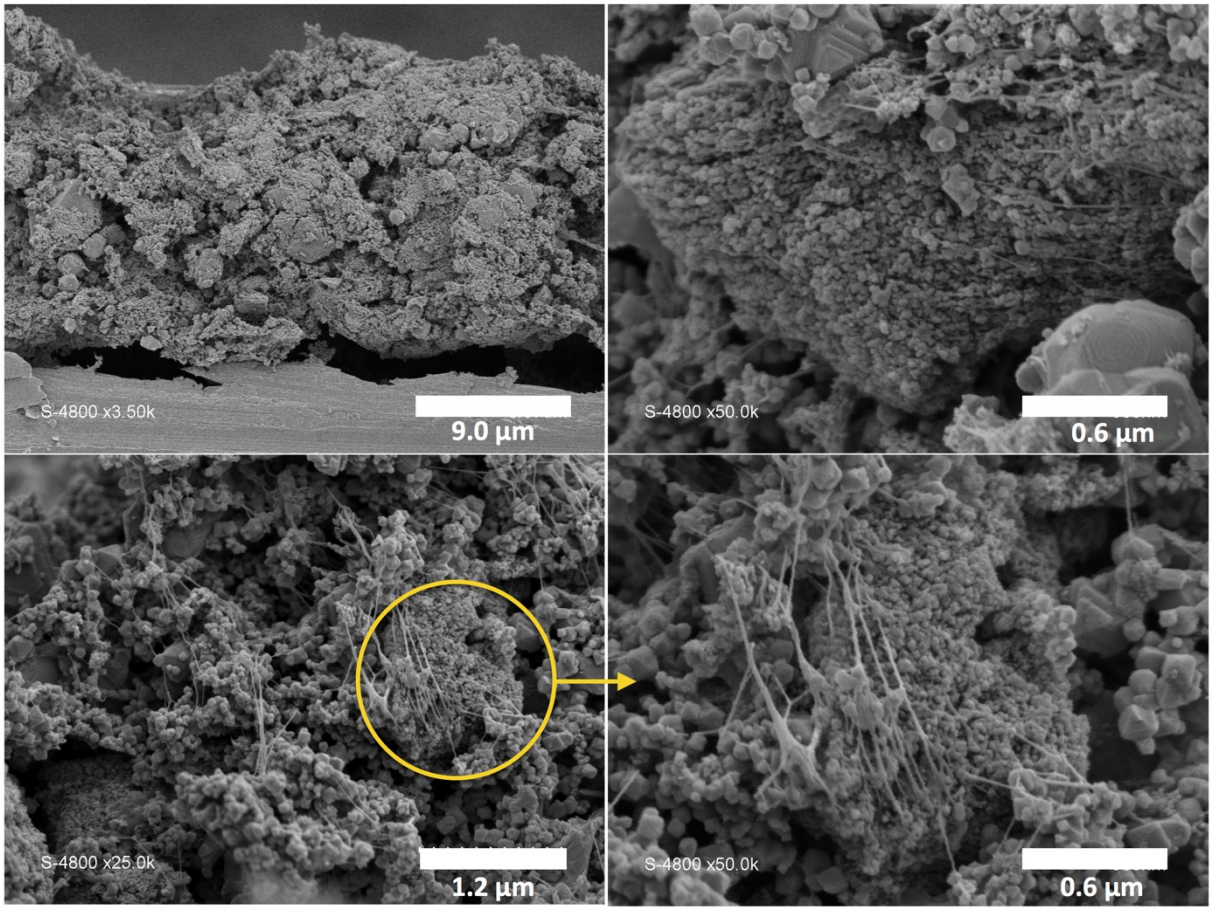

Fig. S11. Additional cross sectional images of LTO-A800HPV electrode

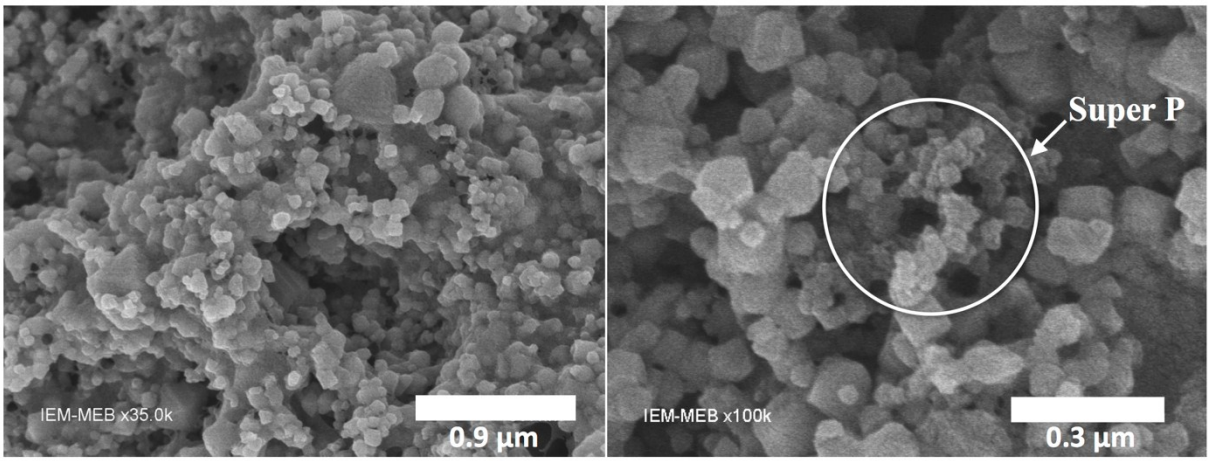

Fig. S12. SEM image (top-view) of LTO-Super P electrode

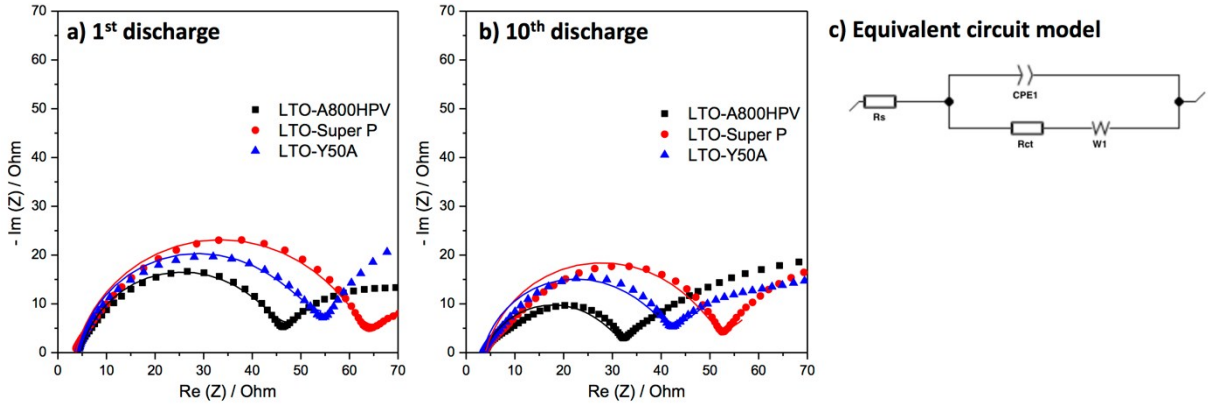

Fig. S13. The Nyquist plots of LTO-A800HPV, LTO-Super P and LTO-Y50A obtained on a) 1st discharge at 58 mA g^{-1}, b) 10th discharge at 58 mA g^{-1} and c) equivalent circuit model used for the fitting. The solid lines represent the fitted data. The fitting was performed until the first semi-circle of each curve. Impedance parameters were given in Table S2.

Sample	Cycle	R_s (Ω)	R_{ct} (Ω)	σ_w (Ω cm^2 $s^{-1/2}$)	D_{Li} (cm^2 s^{-1})
LTO-A800HPV	1st discharge	3.9	43.0	34.6	2.14×10^{-13}
	10th discharge	3.6	29.3	16.5	9.43×10^{-13}
LTO-Super P	1st discharge	3.5	61.6	19.3	6.89×10^{-13}
	10th discharge	3.9	45.6	17.5	8.39×10^{-13}
LTO-Y50A	1st discharge	4.2	47.6	81.5	3.86×10^{-14}
	10th discharge	4.1	36.8	42.4	1.42×10^{-13}

Table S2 Impedance parameters for LTO-A800HPV, LTO-SuperP and LTO-Y50A. R_s(Ω) stands for the ohmic resistance from the entire system such as the electrolyte, the cables, any copper wire placed between the connectors of the instrument, R_{ct} for the charge transfer resistance, σ_w for Warburg impedance coefficient and D_{Li} for the lithium diffusion coefficient.

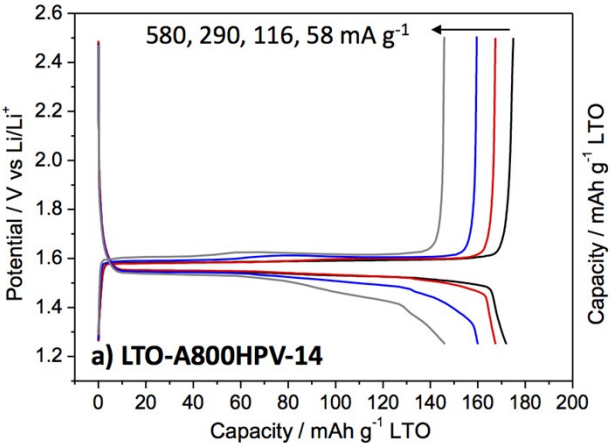
580, 290, 116, 58 mA g-1
Potential / V vs Li/Li+
Capacity / mAh g-1 LTO
a) LTO-A800HPV-14

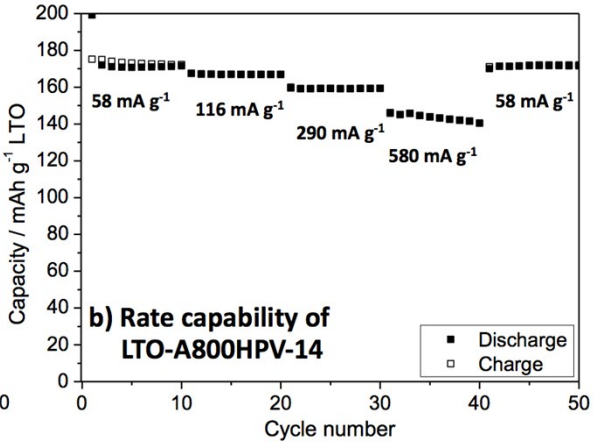
58 mA g-1
116 mA g-1
290 mA g-1
580 mA g-1
58 mA g-1
Capacity / mAh g-1 LTO
Cycle number
b) Rate capability of
LTO-A800HPV-14
Discharge
Charge

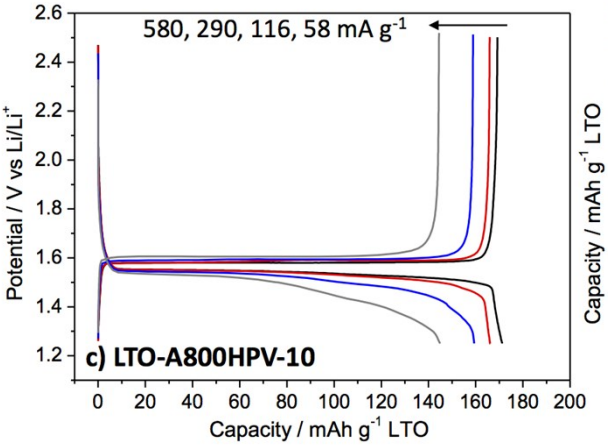
580, 290, 116, 58 mA g-1
Potential / V vs Li/Li+
Capacity / mAh g-1 LTO
c) LTO-A800HPV-10

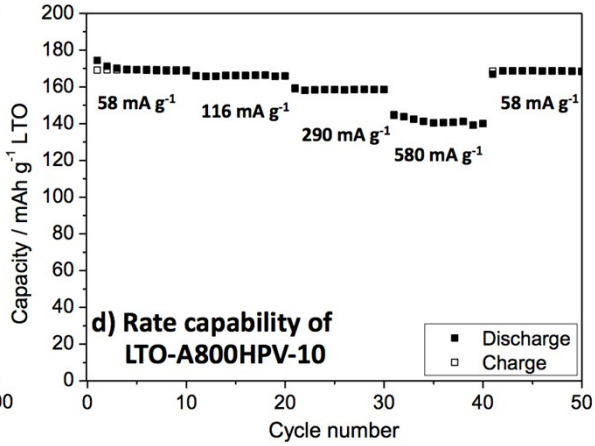
58 mA g-1
116 mA g-1
290 mA g-1
580 mA g-1
58 mA g-1
Capacity / mAh g-1 LTO
Cycle number
d) Rate capability of
LTO-A800HPV-10
Discharge
Charge

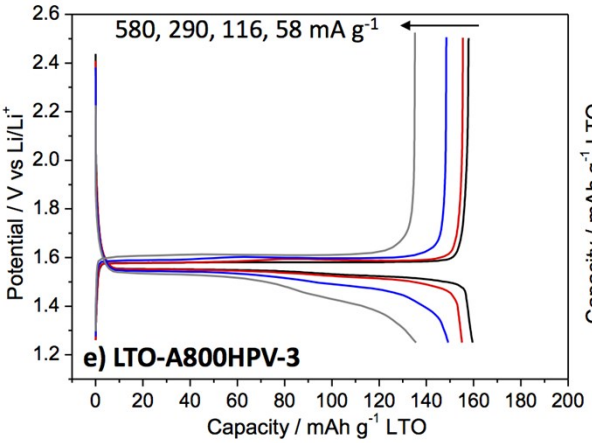
580, 290, 116, 58 mA g-1
Potential / V vs Li/Li+
Capacity / mAh g-1 LTO
e) LTO-A800HPV-3

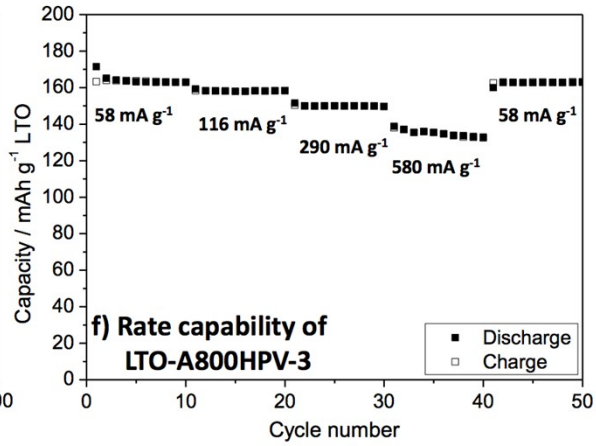
58 mA g-1
116 mA g-1
290 mA g-1
580 mA g-1
58 mA g-1
Capacity / mAh g-1 LTO
Cycle number
f) Rate capability of
LTO-A800HPV-3
Discharge
Charge

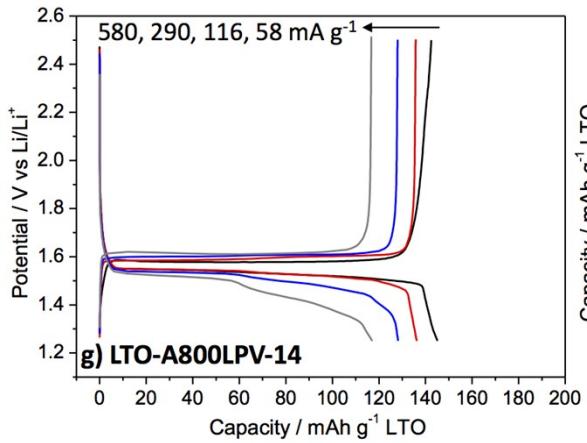
580, 290, 116, 58 mA g-1
Potential / V vs Li/Li+
Capacity / mAh g-1 LTO
g) LTO-A800LPV-14

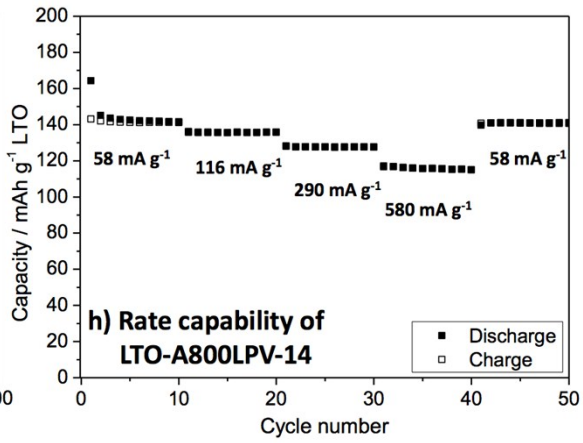
58 mA g-1
116 mA g-1
290 mA g-1
580 mA g-1
58 mA g-1
Capacity / mAh g-1 LTO
Cycle number
h) Rate capability of
LTO-A800LPV-14
Discharge
Charge

Fig. S14. Galvanostatic charge-discharge voltage profile of a) LTO-A800HPV-14 (14 wt.% of A800HPV), c) LTO-A800HPV-10, e) LTO-A800HPV-3 and g) LTO-A800LPV-14; b), d), f) and h) their rate-capability / cycling performances at different current density.

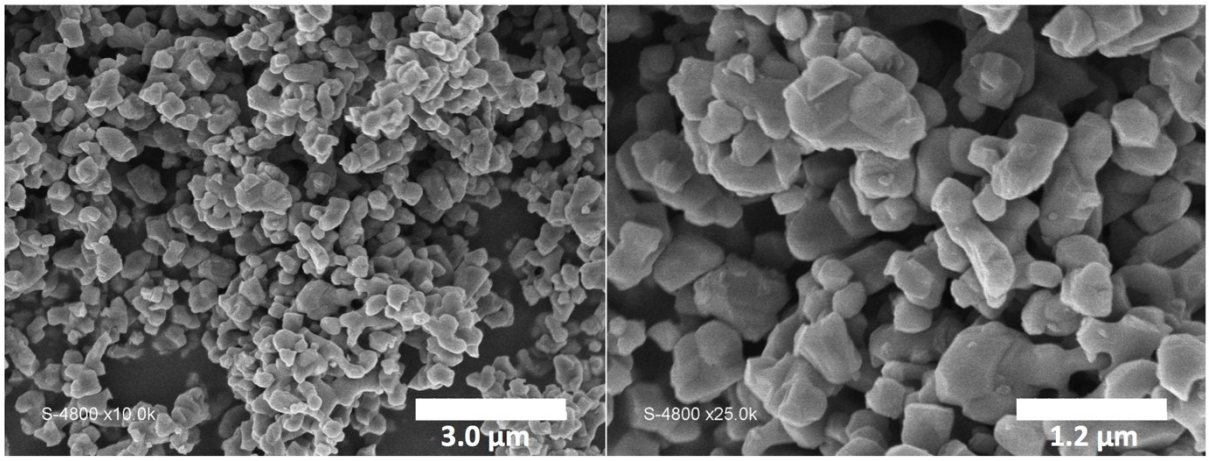

Fig. S15. SEM images of sub-micron sized LTO powder

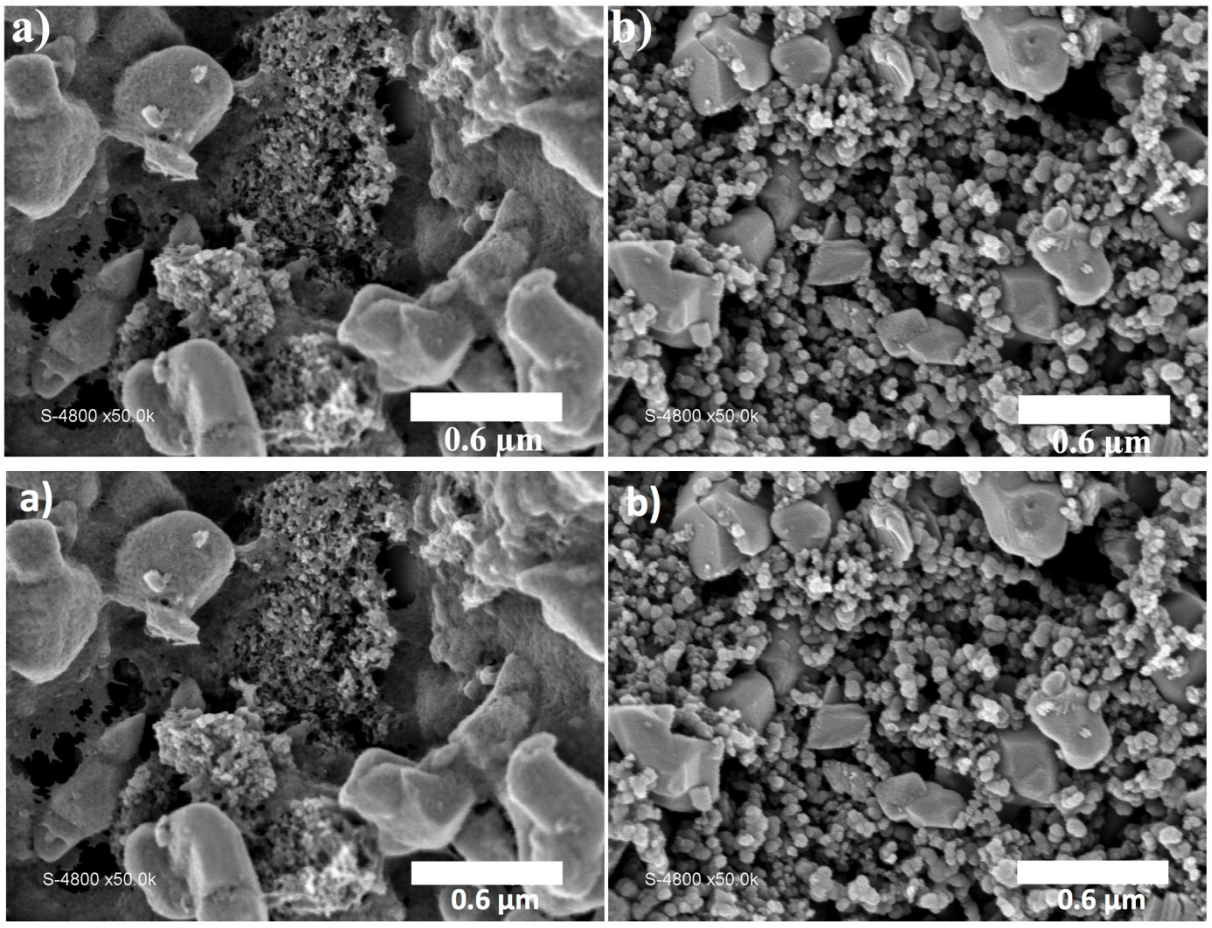

Fig. S16. SEM image (top-view) of a) sub-micron sized LTO-A800HPV electrode and b) sub-micron sized LTO-Super P electrode

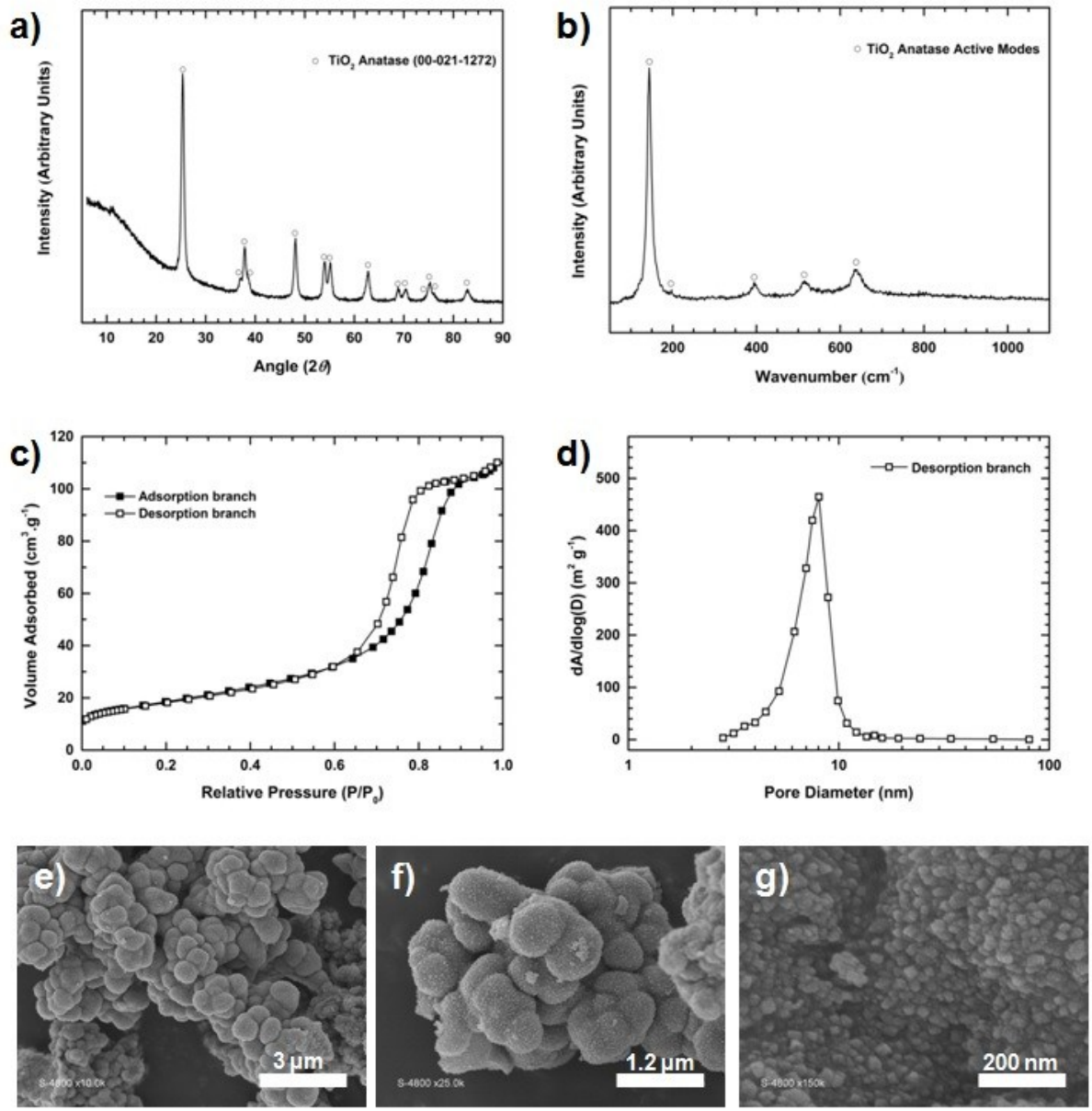

Fig. S17. Characterizations of data of mesoporous TiO_2: a) XRD pattern, b) Raman spectra, c) N_2 adsorption-desorption isotherm, d) BJH pore size distribution (desorption branch) and (e-g) SEM micrographs at different magnifications.

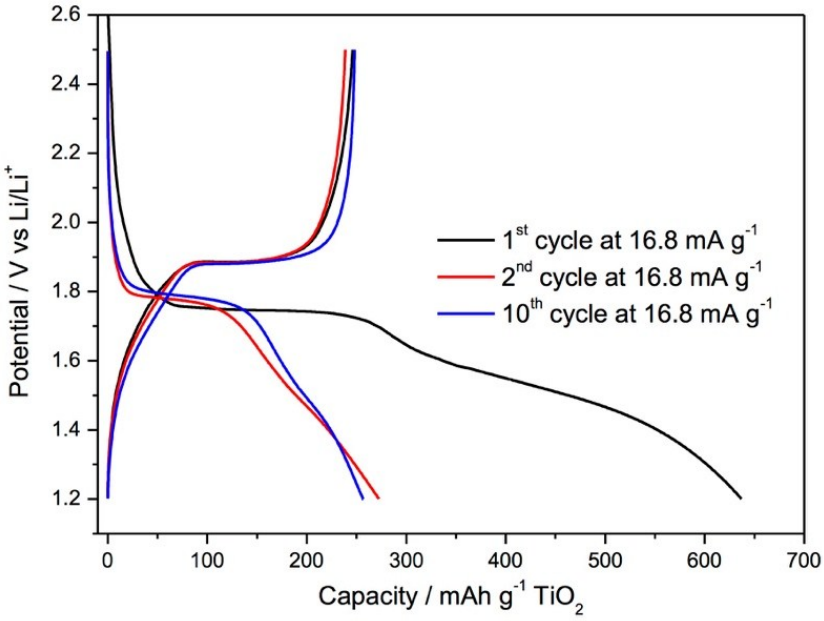

Fig. S18. Galvanostatic charge-discharge voltage profile of TiO_2-A800HPV electrode for 1st, 2nd and 10th cycle at 16.8 mA g^{-1}